


Article

Phase-Only Pattern Synthesis for Spaceborne Array Antenna Based on Improved Mayfly Optimization Algorithm

Hongming Hu ^{1,2,*} , Huawang Li ^{1,2,3}, Guang Liang ^{1,2,3}, Lulu Zhao ^{1,2}, Jiashuo Yang ^{1,2} and Xiaoli Wei ^{1,2}

¹ Innovation Academy for Microsatellite of CAS, Shanghai 201204, China

² University of Chinese Academy of Sciences, Beijing 100049, China

³ Shanghai Engineering Center for Microsatellites, Shanghai 201204, China

* Correspondence: huhm@microsat.com

Abstract: A new optimization algorithm—Improved Mayfly Optimization Algorithm (IMOA)—is proposed in this paper to fulfill the low sidelobe level (SLL) design requirements of the spaceborne array antenna. MOA is a new heuristic algorithm inspired by the flying behavior and mating process of mayflies. It has a unique speed updating system with great convergence, strong stability, fast solution speed, and high precision. Based on the MOA, IMOA not only introduces the adaptive inertial weight factor to enhance the search ability, but also uses the Levy flight strategy and the golden sine operator to improve the disadvantage of easily falling into the local optimal solution. Firstly, according to the antenna pattern requirements of high gain and low sidelobe, an optimization problem model is carried out. Then, the IMOA is applied to solve the problem by only controlling the phase under a given secondary amplitude distribution. Simulation results show that IMOA has great advantages in the maximum sidelobe level (MSLL) suppression and convergence speed. Finally, the EM simulations are conducted on the 528-element planar array antenna. The maximum sidelobe level suppression performances in the test are very consistent with the theoretical simulation, which verifies the feasibility and effectiveness of the proposed IMOA.

Keywords: antenna arrays; antenna pattern synthesis; low sidelobe; mayfly optimization algorithm



Citation: Hu, H.; Li, H.; Liang, G.; Zhao, L.; Yang, J.; Wei, X. Phase-Only Pattern Synthesis for Spaceborne Array Antenna Based on Improved Mayfly Optimization Algorithm. *Electronics* **2023**, *12*, 895. <https://doi.org/10.3390/electronics12040895>

Academic Editor: Reza K. Amineh

Received: 10 January 2023

Revised: 5 February 2023

Accepted: 7 February 2023

Published: 9 February 2023



Copyright: © 2023 by the authors. Licensee MDPI, Basel, Switzerland. This article is an open access article distributed under the terms and conditions of the Creative Commons Attribution (CC BY) license (<https://creativecommons.org/licenses/by/4.0/>).

1. Introduction

The spaceborne antenna array has attracted increased attention in recent years due to its excellent beamforming, beam steering, and high gain characteristics. The fundamental concern in the synthesis of array antenna patterns is to find an adequate excitation amplitude and phase to create the required radiation pattern. To handle the complex antenna pattern synthesis problem, many approaches, including traditional mathematical methodologies and optimization algorithms, have been developed [1–4]. One of the most important technical indications in antenna design synthesis is the sidelobe level. An antenna pattern with a low sidelobe level can significantly increase communication quality by boosting the signal-to-noise ratio, decreasing the influence of the clutter signal outside the main beam, and improving the overall system's anti-interference performance [5–8]. Controlling the excitation amplitude of an antenna element in a large-scale array antenna requires a corresponding feed network, which is hard and expensive. However, phase weighting simply requires the phase shifter, which is simple and inexpensive. As a result, using phase-only weighting for array antenna pattern synthesis is frequently requested to simplify the complexity of the array feeding network and minimize manufacturing costs [9,10].

Genetic Algorithm (GA) and Particle Swarm Optimization (PSO) are the first two popular and classical optimization algorithms, which have been successfully applied to antenna pattern synthesis due to their high efficiency and simplicity [11–14]. However, these two algorithms have the disadvantage of premature convergence when solving multi-parameter optimization problems. Therefore, more and more improved algorithms based

on the classic GA and PSO have been proposed [15,16], such as Differential Evolution Algorithm (DE) [17], Moth Flame Optimization Algorithm (MFO) [18], Fruit-Fly Optimization Algorithm (FOA) [19], Invasive Weed Optimization Algorithm (IWO) [20], Grey Wolf Optimization Algorithm (GWO) [21], Mayfly Algorithm (MA) [22], Compressed Sensing (CS) [23], Biogeography-Based Optimization (BBO) [24], Firefly Algorithm (FA) [25], Ant Colony Optimization (ACO) [26], and so on. Although above algorithms can achieve good results in array antenna synthesis, further improvement is still needed. When the number of antenna elements increases, too many parameters will lead to slow calculation speed and low efficiency of the algorithm, and their solutions will easily fall into the local optimal solution.

Mayfly Optimization Algorithm (MOA) is a new intelligent optimization algorithm proposed by Zervoudakis and Tsafarakis in 2020 [27], which was inspired by the flying behavior and mating process of mayflies, including the mayfly crossing, mutation, group gathering, wedding dance, and random walking operations. Due to its unique speed updating system, MOA has the advantages of strong stability, fast solution speed, and high precision.

In 2021, Owoola applied the MOA to pattern synthesis of uniform and sparse linear antenna array to reduce side lobes [28]. An Improved Mayfly Optimization Algorithm (IMOA) is suggested in this study and used for the antenna pattern synthesis of low sidelobe planar arrays to increase the global search ability and solution accuracy of the MOA. The IMOA is offered as an alternative to the regular MOA. On the one hand, an adaptive inertial weight factor is used to improve the algorithm's search ability; on the other hand, the Levy flight strategy and the golden sine factor are introduced to address the shortcoming of being easily trapped in the local optimal solution, which increases population diversity and speeds up convergence. This work compares the IWOA to various algorithms and uses numerous common test functions to demonstrate its advantages in terms of convergence speed and solution correctness. Finally, the suggested IMOA is applied to an antenna synthesis model developed within the restrictions of the practical engineering project in order to meet the design objectives of high gain and low sidelobe. With a particular secondary amplitude distribution, IMOA estimates the phase excitation of each antenna element. By comparing the results of experiments and simulations, the superiority and effectiveness of the proposed IMOA in the synthesis of space-borne planar array antennas are demonstrated.

The sections of this paper are organized as follows: Section 2 introduces the mayfly optimization algorithm. Section 3 explains the improved mayfly optimization algorithm (IMOA) in detail in three aspects. Section 4 analyzes the performance comparison between IMOA and other algorithms. Section 5 gives the results of the related experiments. Section 6 concludes this paper overall.

2. Mayfly Optimization Algorithm

The Mayfly algorithm, a novel form of intelligent optimization algorithm, offers significant optimization ability and research value. It is inspired by mayfly mating activity. The optimal male and female mayfly individuals are mated to produce the optimal progeny during mating behavior. Similarly, suboptimal people are paired to produce suboptimal offspring, and so on. This process follows the rule of survival of the fittest, eventually phasing out those with inferior fitness.

Suppose the positions of the male and female mayflies in the d -dimensional space are $x = (x_1, x_2, x_3, \dots, x_d)$; then, the fitness function value $f(x)$ can be calculated by the position information. Assuming that the speed of the mayfly individual in the dimensional space is $v = (v_1, v_2, v_3, \dots, v_d)$, the flight direction of each mayfly is a dynamic interaction between individual and social flight experience, and both male and female individuals have the best position $pbest$.

2.1. Movement of Male Mayfly

Male mayflies tend to congregate in groups, and each male mayfly's location is altered based on its own and adjacent experience. Let x_i^t be the current position of the mayfly i at the t th iteration, and v_i^t be the speed of the mayfly i at the t th iteration; the expression for updating the position is:

$$x_i^{t+1} = x_i^t + v_i^{t+1} \quad (1)$$

Considering the mayfly's constant movement and the dancing performance at a distance above the water, its speed is updated as:

$$v_{ij}^{t+1} = v_{ij}^t + a_1 e^{-\beta r_p^2} (pbest_{ij} - x_{ij}^t) + a_2 e^{-\beta r_g^2} (gbest_j - x_{ij}^t) \quad (2)$$

where v_{ij}^t is the speed of the mayfly i in the t th iteration in the dimension j ; x_{ij}^t is the position of the mayfly i in the t th iteration of the dimension j , a_1 and a_2 are the attraction coefficients of the mayflies' swimming behavior; $pbest$ is the best position in history, $gbest$ is the global optimal position; β is the visibility coefficient, which is used to control the visible range of the mayfly, r_p represents the distance between the current position and $pbest$, and r_g is the distance between the current position and $gbest$. The distance calculation formula is:

$$\|x_i - X_i\| = \sqrt{\sum_{j=1}^n (x_{ij} - X_{ij})^2} \quad (3)$$

The best mayflies have to continue to perform their distinctive up-and-down dance to obtain the optimal position; therefore, the best mayflies must change speed constantly. Its speed is updated as:

$$v_{ij}^{t+1} = v_{ij}^t + d \cdot r \quad (4)$$

where d represents the dance coefficient, and $r \in [-1, 1]$ is a random coefficient.

2.2. Movement of Female Mayfly

Female mayflies and male mayflies differ in that male mayflies congregate, whereas female mayflies do not. Female mayflies, on the other hand, will fly to mate with male mayflies. Assuming that y_i^t is the position of the female mayfly i in the t th iteration, its position update is expressed as:

$$y_i^{t+1} = y_i^t + v_i^{t+1} \quad (5)$$

The speed of the female mayfly is updated as follows:

$$v_{ij}^{t+1} = \begin{cases} v_{ij}^t + a_2 e^{-\beta r_m^2 (x_{ij}^t - y_{ij}^t)} & \text{if } f(y_i) > f(x_i) \quad (6a) \\ v_{ij}^t + fl \cdot r & \text{if } f(y_i) \leq f(x_i) \quad (6b) \end{cases}$$

where v_{ij}^t represents the speed of the mayfly, y_{ij}^t represents the position of the mayfly, r_m represents the distance between the male and the female mayfly, and fl is the random walk coefficient, which only works when the female mayfly is under no attack.

2.3. Mayfly Mating

Mating between male and female individuals is a trait of all living things, including mayflies. The mating procedure is as follows: two parents are chosen at random from male and female populations, and the method of selecting male and female samples is the same as that of a male enticing a female.

The optimal male mayfly individual is paired with the optimal female mayfly individual in this method, and the suboptimal male mayfly individual is mated with the subpar female mayfly individual. Following mating, the ideal and suboptimal offspring are as follows:

$$offspring1 = L \cdot male + (1 - L) \cdot female \quad (7)$$

$$offspring2 = L \cdot female + (1 - L) \cdot male \quad (8)$$

where $L \in [-1, 1]$.

3. Improved Mayfly Optimization Algorithm

The standard MOA algorithm has better convergence speed and solution accuracy than other swarm intelligence optimization algorithms, but the overall convergence effect and search accuracy can be further improved. Therefore, this paper proposes the IMOA to optimize and improve the strategy from the following three aspects.

3.1. Adaptive Weight

The concept of inertia weight initially appeared in the particle swarm method, which indicates that, in the iteration of particle swarm optimization, the change of particle coordinates is proportional to inertia weight. In this paper, a nonlinear inertial weighting factor is inspired by this. When the inertia weight is high, the algorithm has a strong search ability and will explore a larger region; when the inertia weight is low, the algorithm has a strong late search ability and will search only around the ideal solution. The formula for adaptive inertia weight is as follows:

$$w = \sin\left(\frac{\pi \cdot t}{2 \cdot it_{\max}}\right) + 1 \quad (9)$$

where t is the current iteration number, and it_{\max} is the maximum iteration number. The position update of the male mayfly in MOA after introducing the inertial weight factor is:

$$x_i^{t+1} = wx_i^t + v_i^{t+1} \quad (10)$$

The position update expression of the female mayfly is:

$$y_i^{t+1} = wy_i^t + v_i^{t+1} \quad (11)$$

After integrating adaptive weights, the position update operation will dynamically alter the weights based on the number of iterations, considerably improving the algorithm's overall search ability.

3.2. Levy Flight Strategy

The Levy distribution is a non-Gaussian random process proposed by French mathematician Levy [29]. Levy flight is a random walking pattern that follows the Levy distribution. When walking in a multidimensional space, Levy flight has isotropic random directions. The mayfly's position and speed during flight are likewise fully random, and the mayfly's flight step length when foraging and attracting the opposite sex roughly obeys the Levy distribution, so it can be compared to the Levy flight model.

In the process of finding the best answer, the MOA method is prone to falling into the local optimal value. The Levy flight strategy is implemented into the male mayfly's speed update operation to make the solution hunting process more active and varied. The male mayfly's revised speed update formula is as follows:

$$v_{ij}^{t+1} = v_{ij}^t + a_1 e^{-\beta r_p^2} (Levy \oplus pbest_{ij} - x_{ij}^t) + a_2 e^{-\beta r_s^2} (gbest_j - x_{ij}^t) \quad (12)$$

where $Levy$ represents the Levy flight factor. The expression of the Levy distribution is:

$$Levy(s, \lambda) \approx s^{-\lambda} \quad (13)$$

where s is a random step size; λ is a random number of $(1, 3]$.

3.3. Golden Sine Factor

The Golden Sine Algorithm is introduced in 2017 as a new meta-heuristic algorithm that exploits the link between the sine function and the unit circle in mathematics for

computational iterative optimization [30]. After introducing the golden section number, the solution space can be reduced during the location updating process, and then the area that may generate the ideal solution will be sought, which can considerably enhance search efficiency and achieve a better balance between search and development.

The core of the Golden Sine Algorithm is its position update formula. First, s individuals are randomly generated. The position of the i th ($i = 1, 2, 3, \dots, s$) individual in the d dimension solution space in the t th iteration is $X_i^t = (X_{i1}, X_{i2}, \dots, X_{id})$, and $P_i^t = (P_{i1}, P_{i2}, \dots, P_{id})$ represents the optimal position of the t th generation individual. Then, each individual is updated using the following formula:

$$X_i^{t+1} = X_i^t |\sin(r_1)| + r_2 \sin(r_1) |c_1 \cdot P_i^t - c_2 \cdot X_i^t| \quad (14)$$

$$c_1 = a \cdot \tau + b \cdot (1 - \tau) \quad (15)$$

$$c_2 = a \cdot (1 - \tau) + b \cdot \tau \quad (16)$$

$$\tau = \frac{\sqrt{5} - 1}{2} \quad (17)$$

where r_1 and r_2 are random numbers, $r_1 \in [0, 2\pi]$, $r_2 \in [0, \pi]$, c_1 and c_2 are coefficients calculated through the golden ratio, which can drive the search agent closer to the target value, and a and b are the initial values of the golden section. The golden sine is divided into standard sine intervals, where the period of the sine function is 2π . In order to enable the population to traverse the searched space of each dimension in the entire period, here we take $a = \pi$, $b = -\pi$.

MOA incorporates the golden sine factor to boost search speed. The golden sine section coefficient is employed to generate offspring in the mating and reproduction of mayflies, and the better formula for offspring generation can be stated as:

$$offspring1 = x_i^1 |\sin(r_1)| + r_2 \sin(r_1) |c_1 \cdot pbest_x - c_2 \cdot x_i^t| \quad (18)$$

$$offspring2 = y_i^1 |\sin(r_1)| + r_2 \sin(r_1) |c_1 \cdot pbest_y - c_2 \cdot x_i^t| \quad (19)$$

where $pbest_x$ and $pbest_y$ represent the optimal position under the current number of iterations.

3.4. The Flow of IMOA

The algorithm flow chart of the IMOA is shown in Figure 1.

The pseudo code of IMOA is described in Algorithm 1.

Algorithm 1 improved mayfly optimization algorithm

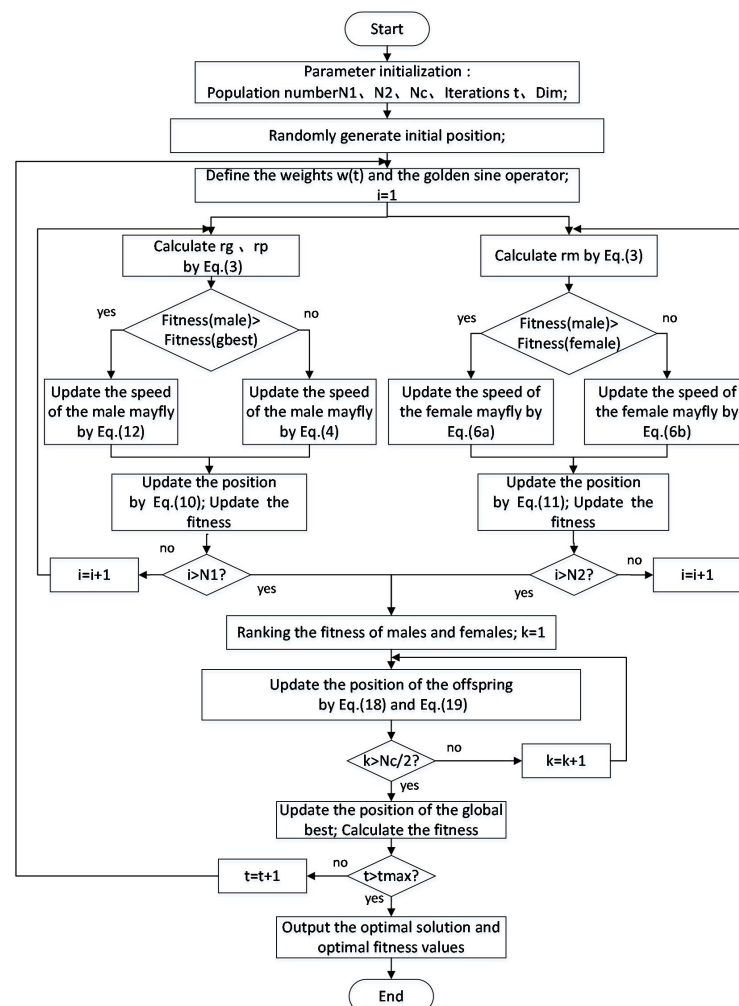
- 1: Parameter initialization: Population number $N1, N2, Nc$, Iterations t, Dim ;
 - 2: Randomly generate initial position X ;
 - 3: $X^* =$ the best search agent;
 - 4: $t = 1$;
 - 5: **while** $t <$ Maximum number of iterations **do**
 - 6: Calculate the fitness of each search agent;
 - 7: Define the weights $w(t)$ and the golden sine operator;
 - 8: $t = 1$;
 - 9: **for** i to $N1$ **do**
 - 10: Update r_g, r_p by Equation (3)
 - 11: **if** $\text{Fitness}(\text{male}) > \text{Fitness}(\text{gbest})$ **then**
 - 12: Update the speed of the male mayfly by Equation (12);
 - 13: **else if** $\text{Fitness}(\text{male}) \leq \text{Fitness}(\text{gbest})$ **then**
 - 14: Update the speed of the male mayfly by Equation (4);
 - 15: **end if**
 - 16: Update the position by Equation (10);
 - 17: Update the fitness;
-

Algorithm 1 *Cont.*

```

18: end for
19: for  $i$  to  $N2$  do
20:   Update  $r_m$  Equation (3)
21:   if  $\text{Fitness}(\text{male}) > \text{Fitness}(\text{female})$  then
22:     Update the speed of the female mayfly by Equation (6a);
23:   else if  $\text{Fitness}(\text{male}) \leq \text{Fitness}(\text{female})$  then
24:     Update the speed of the female mayfly by Equation (6b);
25:   end if
26:   Update the position by Equation (11);
27:   Update the fitness;
28: end for
29: Ranking the fitness of males and females;
30:  $k = 1$ ;
31: for  $k$  to  $Nc/2$  do
32:   Update the position of the offspring by Equations (18) and (19);
33: end for
34: Update the position of the global best;
35: Calculate the fitness of each search agent;
36:  $t = t + 1$ ;
37: end while
38: Return  $X^*$ ;

```

**Figure 1.** The flowchart of IMOA.

3.5. Algorithm Complexity Analysis

Assuming that the computation complexity of IMOA is $T(n)$, the dimension of the search space is denoted as D , the number of male mayflies is N_1 , the number of female mayflies is N_2 , the number of offspring is N_3 , and the maximum number of iterations is denoted as T_{\max} . The complexity of the initialization process is $O(1)$, and the time complexity of the standard MOA is $T(n) = O(1 + T_{\max}(N_1D + N_2D + N_3D))$.

IMOA adds adaptive inertia weights, Levy flight strategies, and golden sine factors, so the complexity will increase correspondingly. The complexity of adaptive inertia weight is $O(1)$, the complexity of Levy flight is $O(N_1)$, and the complexity of golden sine factor is $O(1)$. Since the golden sine factor is nested in the mating loop, the time complexity added by IMOA is $O(T_{\max}(1 + N_1 + N_3))$, the complexity after filtering low-order terms is $T(n) = O(T_{\max}(N_1(D + 1) + N_2D + N_3(D + 1)))$. Overall, IMOA has a slight increase in complexity, but not much.

4. Performance Analysis

Because numerous factors must be optimized, reliability analysis is required prior to array antenna pattern synthesis. According to Wolpert's "no free lunch" (NFL) theorem [31], there is no algorithm in the world that can solve all issues in all sectors. As a result, we use four typical test functions to validate the IMOA's efficiency. These four functions are well-known and have served as reference functions for optimization algorithms such as GA and PSO. Table 1 displays the benchmark functions.

Table 1. Test functions and specific information.

| Function Name | Expression | Search Space | Dim | Fmin |
|---------------|---|----------------|-----|----------------|
| Sphere | $F_1 = \sum_{i=1}^d x_i^2$ | $[-10,10]$ | 30 | 0 |
| Rosenbrock | $F_2 = \sum_{i=1}^{d-1} [100(x_{i+1} - x_i^2)^2 + (1 - x_i)^2]$ | $[-30,30]$ | 30 | 0 |
| Quartic | $F_3 = \sum_{i=1}^d ix_i^4 + \text{random}[0,1)$ | $[-1.28,1.28]$ | 30 | 0+random noise |
| Ackley | $F_4 = 20 + e - 20 \exp[-0.2\sqrt{\frac{1}{d} \sum_{i=1}^d x_i^2}] - \exp[\frac{1}{d} \sum_{i=1}^d \cos(2\pi x_i)]$ | $[-32,32]$ | 30 | 0 |

Using the above four standard test functions, the GA, PSO, DE, IWO, WOA, standard MOA, and IMOA are simulated and compared in 30 dimensions. The computed $f(x)$ is defined as the solution's fitness value. In the aforementioned algorithm, the population size is set to 40, and the maximum number of iterations is 500. Table 2 displays the parameters of various algorithms. Furthermore, to eliminate random bias, tests are independently repeated 30 times.

Table 2. Parameter setups of different algorithms.

| Algorithm | Values of the Parameters |
|-----------|---|
| GA [13] | $P_c = 0.8, P_m = 0.08$ |
| PSO [32] | $C1 = 1.5, C2 = 2.0$ |
| DE [15] | $F = 0.5, CR = 0.1$ |
| IWO [33] | $\sigma_{i\text{initial}} = 0.05, \sigma_{i\text{final}} = 0.01$ |
| MOA [20] | $\text{male} = 20, \text{female} = 20, a_1 = 1, a_2 = 1.5, \beta = 2, d = 5$ |
| WOA [26] | $b = 1, r = [0, 1], l = [-1, 1], p = [0, 1]$ |
| IWOA | $\text{male} = 20, \text{female} = 20, a_1 = 1, a_2 = 1.5, \beta = 2, d = 5, a = \pi, b = -\pi$ |

Table 3 displays the numerical statistical findings of 30 independent experiments calculated using various techniques. The three statistical indicators are ideal value, average value, and variance, which are used to assess the algorithm's optimization accuracy, average

accuracy, and robustness, in that order. The best outcomes are indicated in bold for each function. The three IMOAs listed above clearly outperform the other algorithms in solving the four test functions, as seen in Table 3.

Correspondingly, it can be seen from the convergence curves of different algorithms shown in Figure 2a–d that the proposed IMOAs have faster convergence speed and better solution results in solving the above four test functions. However, the performance of the IMOAs in the sidelobe suppression problem for antenna synthesis still needs to be further evaluated.

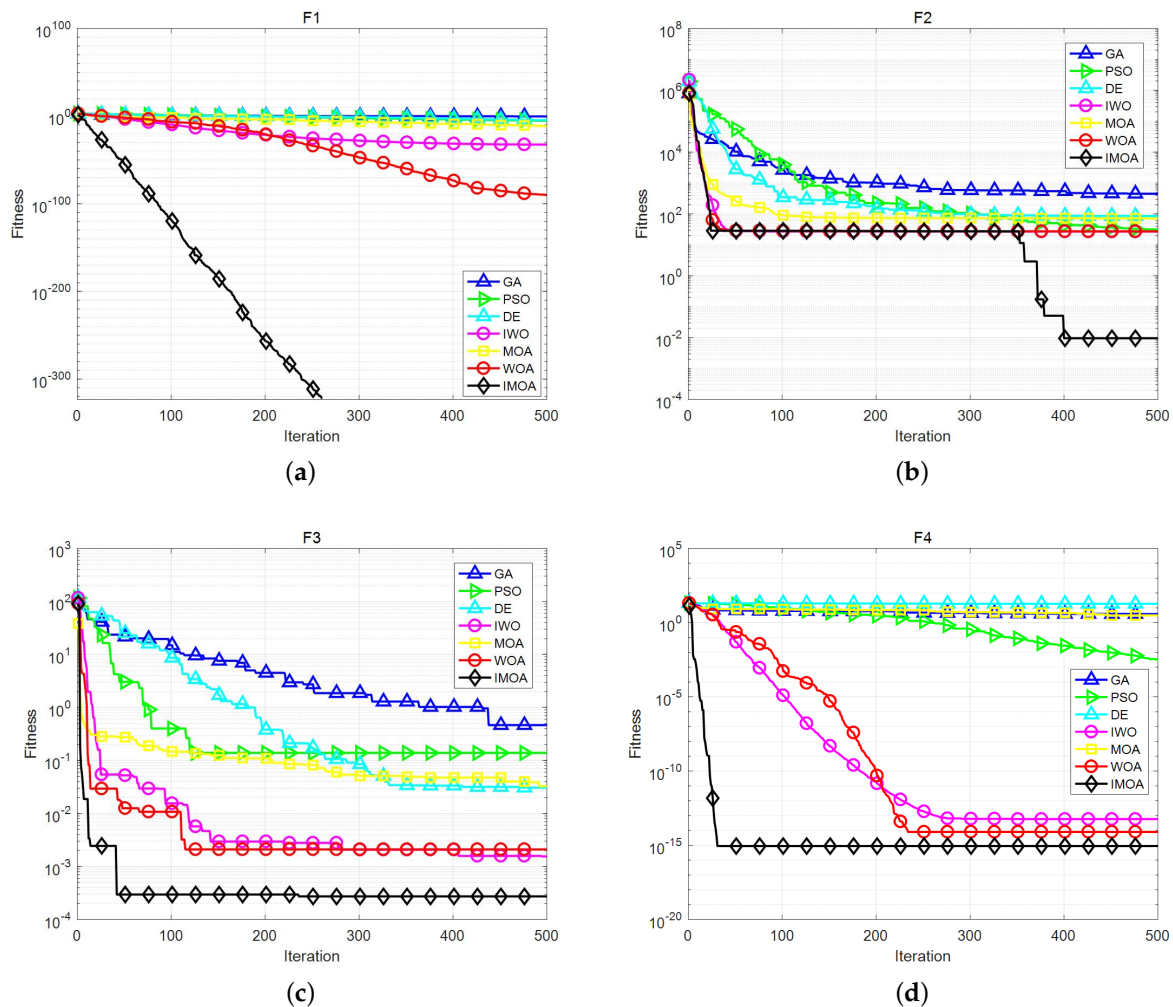


Figure 2. Simulation experiment results. (a) convergence curves of F1; (b) convergence curves of F2; (c) convergence curves of F3; (d) convergence curves of F4.

Table 3. Results of algorithms on basic benchmark functions.

| Function ID | Statistics | GA | PSO | DE | IWO | MOA | WOA | IWOAs |
|-------------|------------|--------------------------|--------------------------|--------------------------|--------------------------|--------------------------|--------------------------|--|
| F1 | Best | 5.9459×10^{-02} | 9.0916×10^{-03} | 1.5094×10^{-06} | 2.5677×10^{-05} | 8.091×10^{-13} | 3.2727×10^{-94} | $0.0000 \times 10^{+00}$ |
| | Average | 1.7310×10^{-01} | 1.6365×10^{-02} | 2.9594×10^{-06} | 3.4267×10^{-05} | 1.674×10^{-10} | 1.2064×10^{-81} | $0.0000 \times 10^{+00}$ |
| | Std. | 2.5419×10^{-01} | 5.2516×10^{-02} | 1.1558×10^{-06} | 4.7039×10^{-06} | 3.7614×10^{-10} | 5.2016×10^{-81} | $0.0000 \times 10^{+00}$ |
| F2 | Best | $2.0635 \times 10^{+02}$ | $2.6832 \times 10^{+01}$ | $2.4624 \times 10^{+01}$ | $2.5779 \times 10^{+01}$ | 3.1467×10^{-01} | $2.6852 \times 10^{+01}$ | 3.2867×10^{-03} |
| | Average | $4.009 \times 10^{+02}$ | $6.3317 \times 10^{+01}$ | $5.2010 \times 10^{+01}$ | $2.6677 \times 10^{+01}$ | $2.4533 \times 10^{+01}$ | $2.7647 \times 10^{+01}$ | 1.2652×10^{-02} |
| | Std. | $1.5590 \times 10^{+02}$ | $3.0563 \times 10^{+01}$ | $3.6656 \times 10^{+01}$ | $0.6031 \times 10^{+00}$ | $2.9960 \times 10^{+01}$ | $0.4685 \times 10^{+00}$ | 2.9483×10^{-03} |
| F3 | Best | 2.4553×10^{-01} | 5.5778×10^{-01} | 6.8942×10^{-02} | 5.7910×10^{-03} | 7.9499×10^{-02} | 3.8572×10^{-03} | 4.5898×10^{-04} |
| | Average | 5.0547×10^{-01} | $1.6257 \times 10^{+00}$ | 1.1957×10^{-01} | 2.6554×10^{-02} | 2.0486×10^{-02} | 3.0396×10^{-02} | 5.2412×10^{-03} |
| | Std. | 1.2738×10^{-01} | 3.8376×10^{-01} | 3.0263×10^{-02} | 8.8917×10^{-02} | 7.7150×10^{-03} | 3.9468×10^{-03} | 8.3869×10^{-04} |
| F4 | Best | 3.2840×10^{-01} | $1.9277 \times 10^{+00}$ | 2.9891×10^{-03} | 3.9968×10^{-14} | 1.2840×10^{-01} | 7.6815×10^{-16} | 8.8818×10^{-16} |
| | Average | 7.3548×10^{-01} | $2.7495 \times 10^{+00}$ | 4.7469×10^{-03} | 5.7495×10^{-14} | 5.2548×10^{-01} | 4.7962×10^{-15} | 8.8818×10^{-16} |
| | Std. | 2.1209×10^{-01} | 5.7580×10^{-01} | 1.0955×10^{-03} | 8.5984×10^{-15} | 3.1209×10^{-01} | 2.158×10^{-15} | $0.0000 \times 10^{+00}$ |

5. Application of IMOA in the Array Antenna Pattern Synthesis

5.1. Signal Model of the Planar Phased Array Antenna

Consider the planar phased array composed of N elements shown in Figure 3, its far-field radiation pattern is:

$$E(\theta, \phi) = \sum_{n=1}^N g(\theta, \phi) w_n^* e^{jk(x_n \sin \theta \cos \phi + y_n \sin \theta \sin \phi)} \quad (20)$$

$$= g(\theta, \phi) \sum_{n=1}^N |w_n| e^{jk(x_n \sin \theta \cos \phi + y_n \sin \theta \sin \phi) + j\varphi_n} \quad (21)$$

where $g(\theta, \phi)$ is the element pattern function, $k = 2\pi/\lambda$, λ is the wavelength, (x_n, y_n) is the coordinate position of the n th array element, and $|w_n| \cdot e^{j\varphi_n}$ is the amplitude excitation factor and phase excitation factor of the corresponding array element.

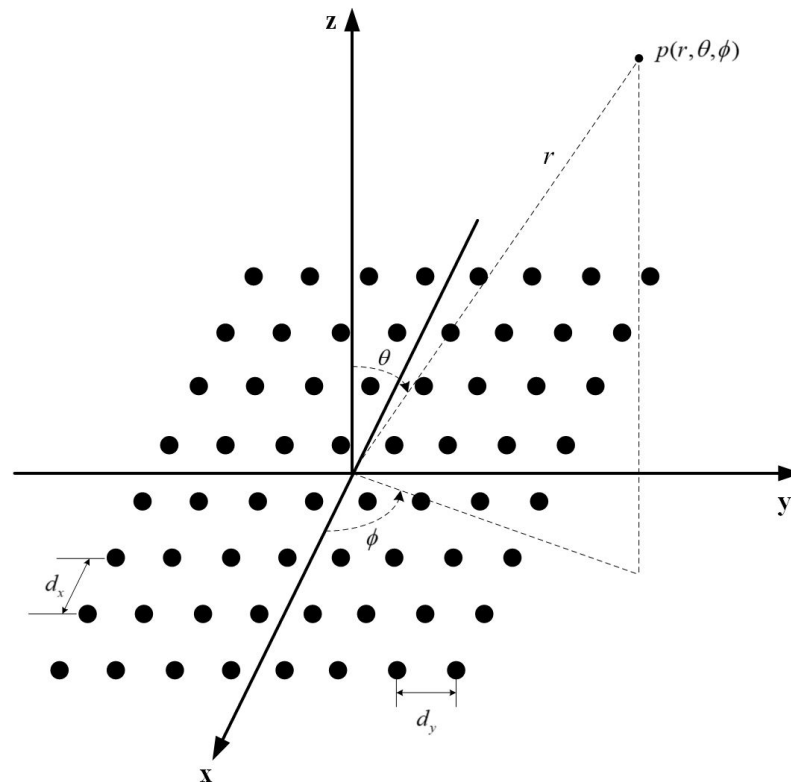


Figure 3. The planar phased array model.

This paper applies the IMOA to actual engineering projects. In large-scale spaceborne array antennas, the method to control the excitation amplitude of the array antenna units by designing the corresponding feed network is complicated, difficult, and expensive. However, phase weighting generally only needs to be controlled by a phase shifter, which is simple and convenient, without additional cost. However, it is difficult to achieve a particularly low sidelobe only through phase modulation. In order to achieve the low sidelobe level, the secondary amplitude distribution is first obtained by binarizing the Taylor distribution; then, the desired sidelobe suppression is achieved only by optimizing the phase of the excitation. The fitness function can be expressed as:

$$F_{MSLL} = \alpha_1 |G_0 - G_{des}| + \alpha_2 |MSLL_{max} - MSLL_{des}| \quad (22)$$

where G_0 is the calculated gain of the mainlobe pointing angle, G_{des} is the designed gain of the mainlobe pointing angle, $MSLL_{max}$ is the calculated maximum sidelobe level among

the entire pattern range, $MSLL_{des}$ is the designed maximum sidelobe level, α_1 and α_2 are two weight coefficients, and $\alpha_1 + \alpha_2 = 1$ in the design.

5.2. Results Analysis

In order to endure high radiation power from the transmitter [34,35], the Tx antenna employs a type of the crossed dipole which is made of copper. Every two opposite arms form a linearly-polarized dipole. Circularly-polarized radiation is realized through adjusting the length of arms of the two dipoles. The antenna is fed by a balun through the open slit which is $1/4$ wavelength. The Simulation Gain is 7.1 dB. The design diagram and radiation pattern of the antenna element are shown as Figures 4 and 5.

In the 528-element planar array antenna model, the secondary amplitude distribution is first obtained by binarizing the Taylor distribution. The secondary amplitude distribution ratio is 1:0.7, which can be seen in Figure 6. The frequency is set to 18.75 GHz, and 528 elements with different unit patterns are imported through the simulation software HFSS. Then, GA, PSO, DE, IWO, WOA, and standard MOA and IMO are carried out to optimize the phase excitation to achieve sidelobe suppression. Figure 7 is the planar array antenna. The parameter design of each algorithm is shown in Table 2. Each algorithm is iterated 2000 times and repeated 20 times independently to ensure the reliability of the experiment. It can be seen from Figure 8 that the IMO is significantly better than other algorithms in terms of convergence speed, and the final solution is also better than other algorithms.

Seven algorithms are selected to solve the problem of sidelobe suppression for phased array antennas, and the corresponding optimal solution of each algorithm is shown in Figure 9. As shown in Figure 9, the maximum sidelobe obtained by IMO optimization is -25.73 dB, and the maximum sidelobe in the conventional pattern without adjusting the phase is -14.98 dB. The obvious optimization proves the superiority of the IMO, which can also be verified by the comparison of 3D antenna pattern in Figure 10.

The optimal value, average value, and variance of 20 independent experiments are shown in Table 4. After IMO optimization, the best MSLL reaches -25.73 dB, the worst MSLL is -24.55 dB, and the standard deviation of 20 experiments is 0.42. It can be seen that the IMO performs better on optimization results and robustness through the comparison with other algorithms in Table 4.

In the simulation model mentioned above, the mutual coupling among the array elements are not taken into account. Therefore, it is necessary to conduct EM simulations to determine whether the above algorithm can effectively optimize the maximum sidelobe of the pattern in the presence of mutual coupling.

The EM simulations are conducted based on ANSYS Electromagnetics (HFSS). The phase excitation obtained through algorithm optimization in MATLAB is input into the 528-element planar array antenna model designed in HFSS software to verify the feasibility of the optimization algorithm in actual engineering. Figure 11 shows the comparison of the 2D beam optimization performance of each algorithm obtained through EM simulation. It can be seen that the MSLL optimized by the IMO is -23.51 dB. Obviously, the MSLL suppression performance of the IMO is the best compared with other algorithms. The sidelobe suppression performance of the HFSS simulation results deteriorate to a certain extent after adding coupling, but both simulations still demonstrate the effectiveness of the IMO.

Furthermore, the 3D waveform diagrams before and after optimization of 528 elements are shown in Figure 12a,b respectively. The color of the largest sidelobe becomes lighter, indicating that the value is significantly smaller, which proves that the maximum SLLs are significantly optimized.

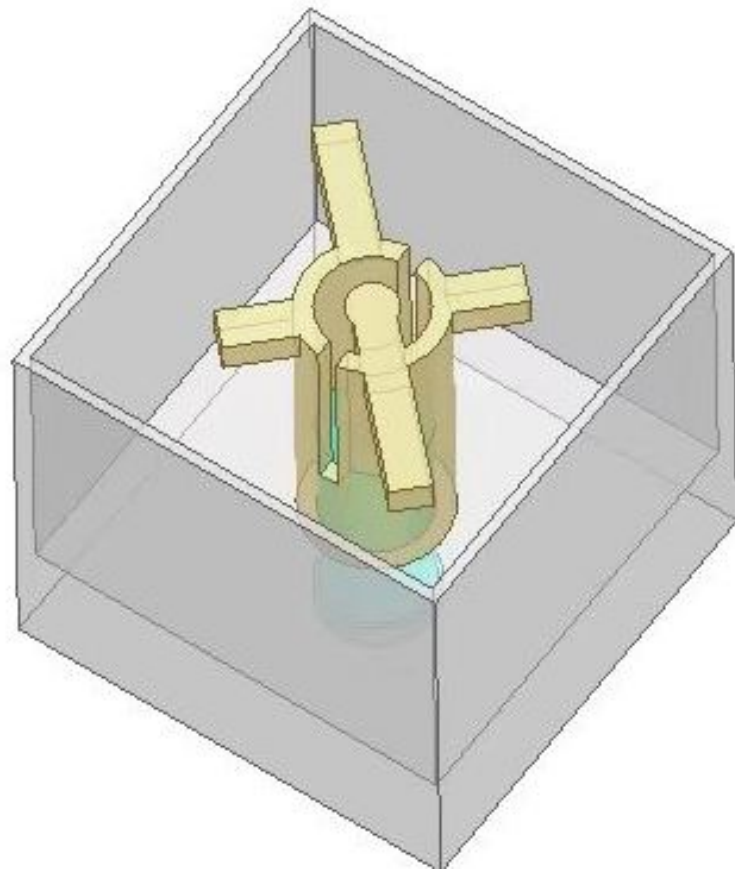


Figure 4. Design diagram of the antenna element.

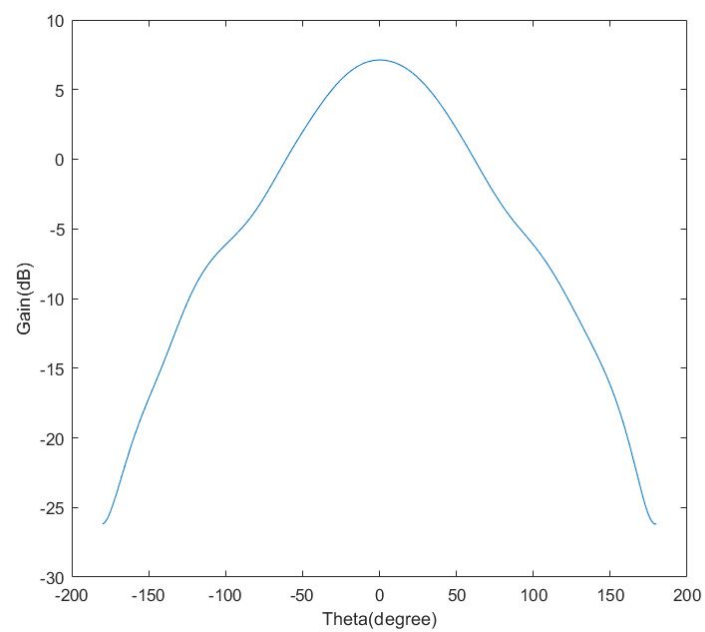


Figure 5. Radiation pattern of the antenna element.

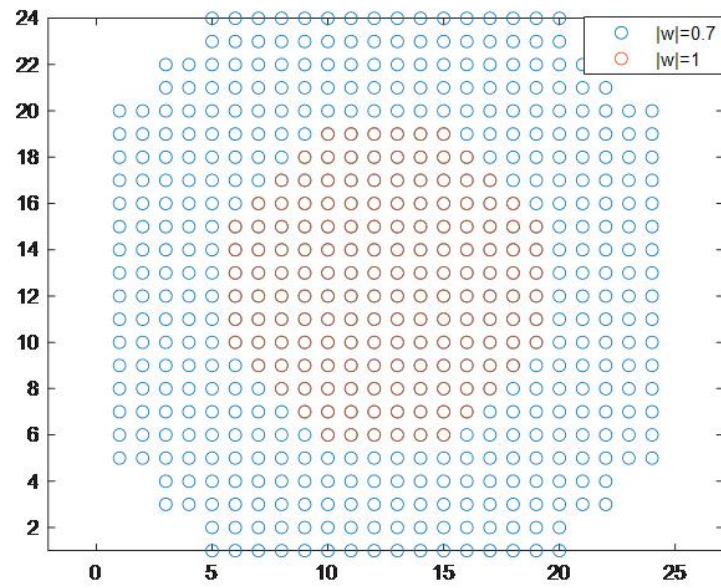


Figure 6. Weights distribution of the array.

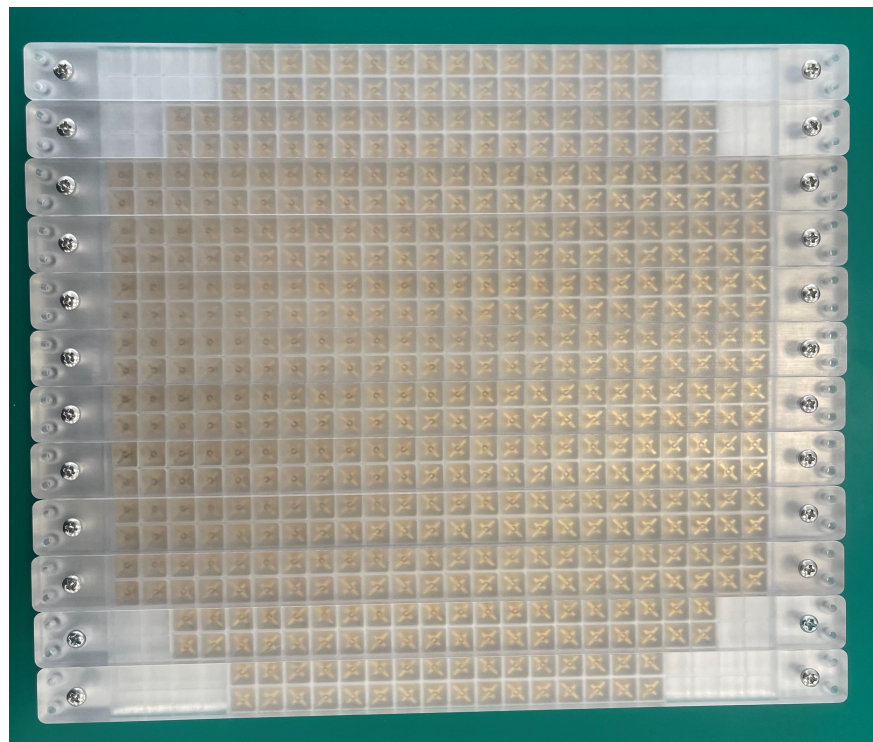


Figure 7. Planar phased array antenna.

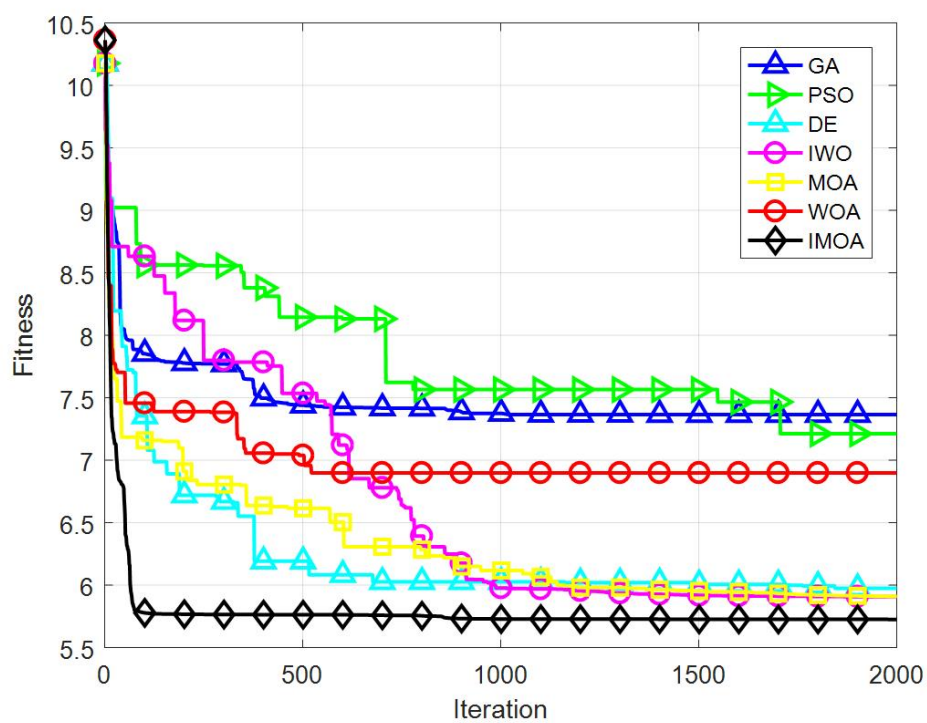


Figure 8. Convergence rates of a 528-element planar phased array.

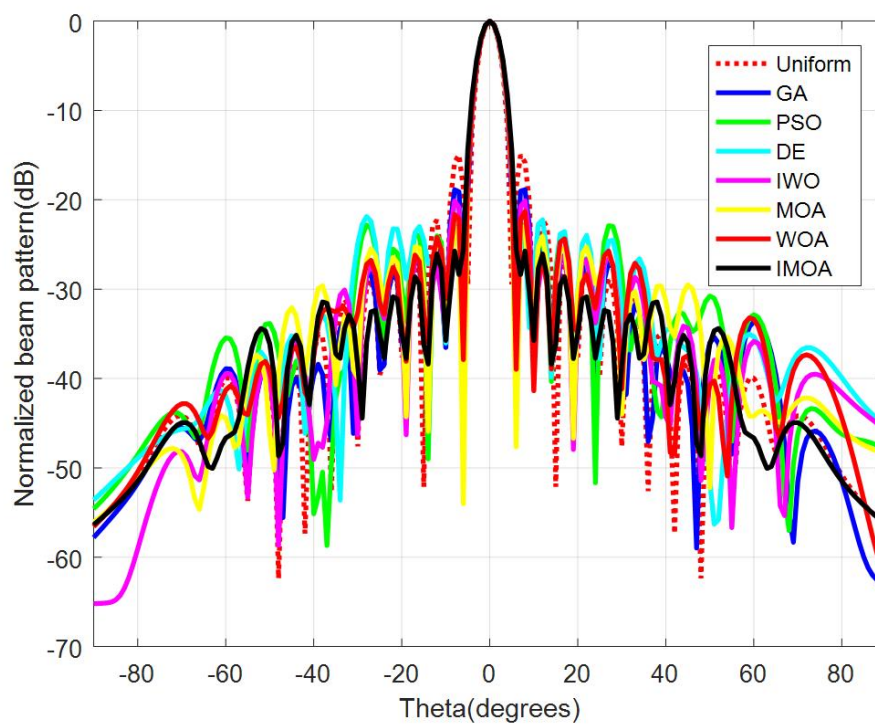


Figure 9. 2D beam patterns of a 528-element planar phased array.

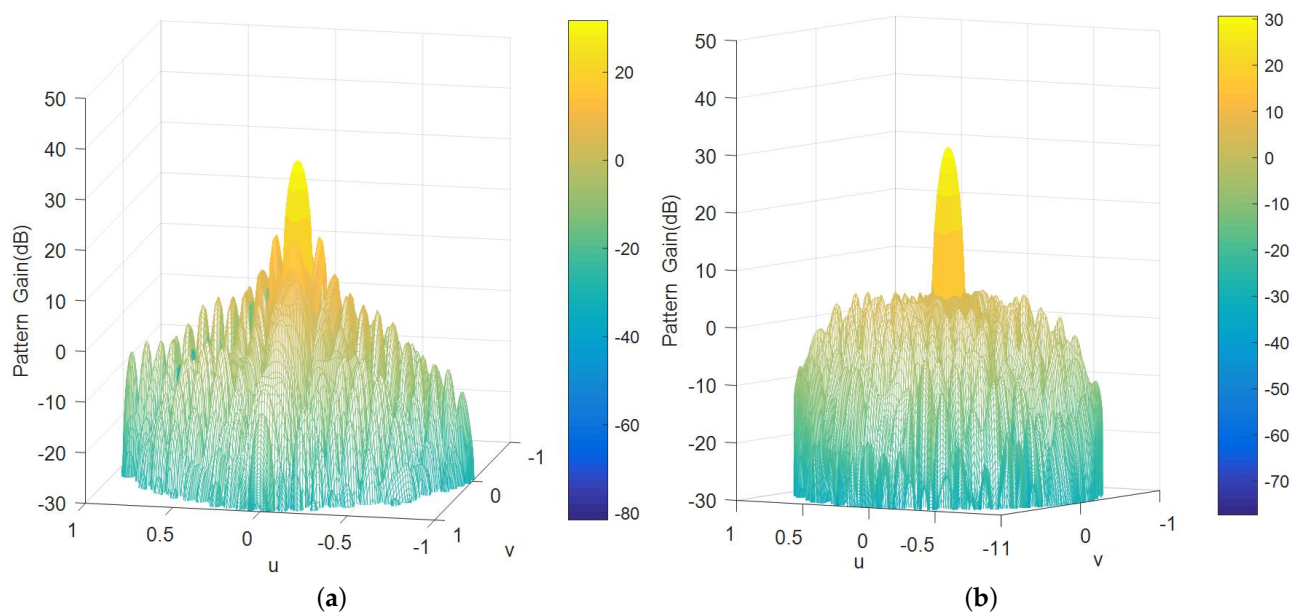


Figure 10. 3D beam patterns of 528-element Planar Phased Array. (a) 3D beam pattern of the uniform 528-element Planar Phased Array; (b) 3D beam pattern of the 528-element Planar Phased Array optimized with IMOA.

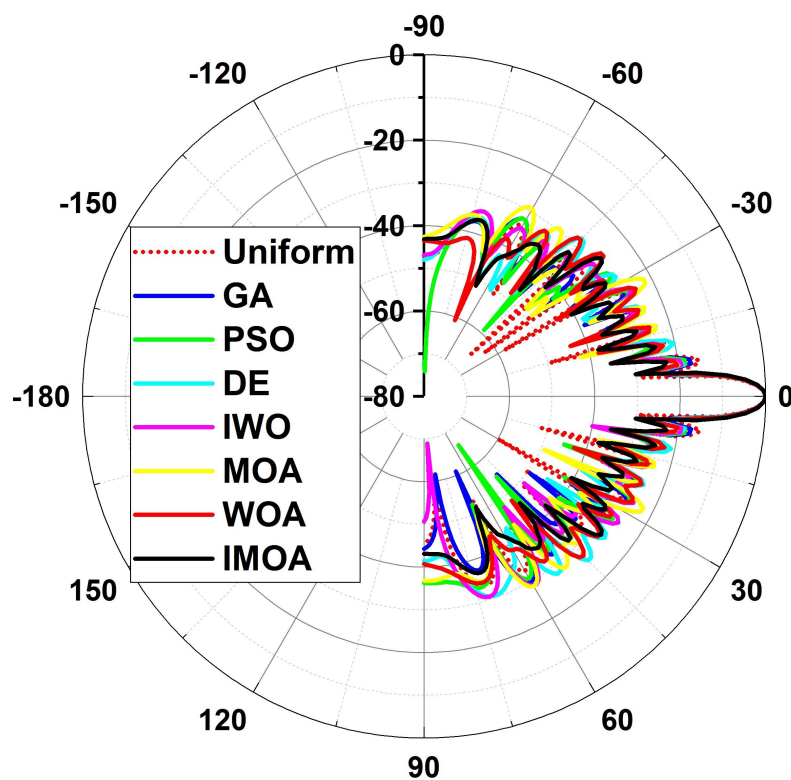
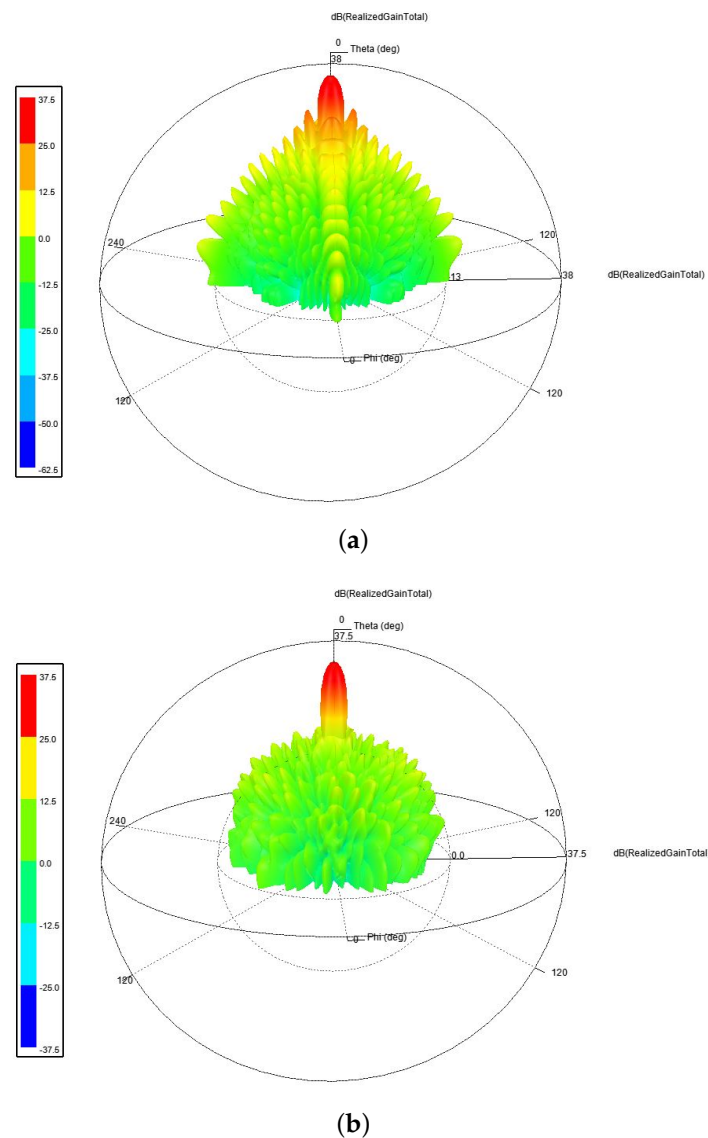


Figure 11. 2D EM simulation results.

Table 4. Results of algorithms on basic benchmark functions.

| Algorithms | Best MSLL (dB) | Worst MSLL (dB) | Average MSLL (dB) | Standard Deviation (dB) |
|---------------|----------------|-----------------|-------------------|-------------------------|
| Uniform Array | −14.98 | −14.98 | −14.98 | 0 |
| GA | −18.87 | −16.95 | −17.68 | 0.77 |
| PSO | −20.13 | −17.86 | −18.89 | 1.32 |
| DE | −20.37 | −18.16 | −19.02 | 0.98 |
| IWO | −21.64 | −20.28 | −20.96 | 0.56 |
| MOA | −23.52 | −21.19 | −22.21 | 1.13 |
| WOA | −23.08 | −21.56 | −22.13 | 0.63 |
| IMOA | −25.73 | −24.55 | −25.26 | 0.42 |

**Figure 12.** Three-dimensional EM simulation results. (a) 3D EM simulation results of the uniform 528-element Planar Phased Array; (b). 3D EM simulation results of the 528-element Planar Phased Array optimized with IMOA.

6. Conclusions

In this paper, an Improved Mayfly Optimization Algorithm (IMOA) is proposed for the low sidelobe design requirements of the spaceborne array antennas. On the basis of the standard MOA, the IMOA has three improvement strategies: adaptive weight, the

Levy flight strategy, and the golden sine operator. The superiority of IMOA is proved by comparing with other algorithms through the classic test function simulations, and the IMOA is successfully applied to the phase-only pattern synthesis of a 528-element planar array antenna. On the maximum sidelobe level suppressing problem, IMOA has better performance than GA, PSO, DE, IWO, WOA, and the standard MOA in terms of convergence speed and the final optimization results. Finally, the practicability and effectiveness of the IMOA are verified through the electromagnetic field simulation with coupling added.

Author Contributions: Conceptualization, H.H., H.L. and L.Z.; Methodology, H.H., H.L. and G.L.; Investigation, H.H. and J.Y.; Supervision, X.W., J.Y. and L.Z.; writing—original draft preparation, H.H. and G.L.; writing—review and editing, L.Z.; project administration, H.H. All authors have read and agreed to the published version of the manuscript.

Funding: This work was supported in part by the National Natural Science Foundation of China (Grant No. U21A20443) and the Shanghai Industrial Collaborative Innovation Project (Grant No. XTCX-KJ-2022-02).

Data Availability Statement: Not applicable.

Conflicts of Interest: The authors declare no conflict of interest.

References

1. Prado, D.R. The Generalized Intersection Approach for Electromagnetic Array Antenna Beam-Shaping Synthesis: A Review. *IEEE Access* **2022**, *10*, 87053–87068. [\[CrossRef\]](#)
2. Ha, B.V.; Mussetta, M.; Pirinoli, P.; Zich, R.E. Modified Compact Genetic Algorithm for Thinned Array Synthesis. *IEEE Antennas Wirel. Propag. Lett.* **2016**, *15*, 1105–1108. [\[CrossRef\]](#)
3. Keizer, W.P.M.N. Low-Sidelobe Pattern Synthesis Using Iterative Fourier Techniques Coded in MATLAB [EM Programmer's Notebook]. *IEEE Antennas Propag. Mag.* **2009**, *51*, 137–150. [\[CrossRef\]](#)
4. Li, H.; Jiang, Y.; Ding, Y.; Tan, J.; Zhou, J. Low-Sidelobe Pattern Synthesis for Sparse Conformal Arrays Based on PSO-SOCP Optimization. *IEEE Access* **2018**, *6*, 77429–77439. [\[CrossRef\]](#)
5. Keizer, W.P.M.N. Amplitude-Only Low Sidelobe Synthesis for Large Thinned Circular Array Antennas. *IEEE Trans. Antennas Propag.* **2012**, *60*, 1157–1161. [\[CrossRef\]](#)
6. Yang, F. Synthesis of Low-Sidelobe 4-D Heterogeneous Antenna Arrays Including Mutual Coupling Using Iterative Convex Optimization. *IEEE Trans. Antennas Propag.* **2020**, *68*, 329–340. [\[CrossRef\]](#)
7. Lin, Z.; Hu, H.; Chen, B.; Lei, S.; Tian, J.; Gao, Y. Shaped-Beam Pattern Synthesis With Sidelobe Level Minimization via Nonuniformly-Spaced Sub-Array. *IEEE Trans. Antennas Propag.* **2022**, *70*, 3421–3436. [\[CrossRef\]](#)
8. Safaai-Jazi, A.; Stutzman, W.L. A New Low-Sidelobe Pattern Synthesis Technique for Equally Spaced Linear Arrays. *IEEE Trans. Antennas Propag.* **2016**, *64*, 1317–1324. [\[CrossRef\]](#)
9. Khalaj-Amirhosseini, M. Phase-Only Power Pattern Synthesis of Linear Arrays Using Autocorrelation Matching Method. *IEEE Antennas Wirel. Propag. Lett.* **2019**, *18*, 1487–1491. [\[CrossRef\]](#)
10. Liang, J.; Fan, X.; Fan, W.; Zhou, D.; Li, J. Phase-Only Pattern Synthesis for Linear Antenna Arrays. *IEEE Antennas Wirel. Propag. Lett.* **2017**, *16*, 3232–3235. [\[CrossRef\]](#)
11. Liang, Z.; Ouyang, J.; Yang, F. A hybrid GA-PSO optimization algorithm for conformal antenna array pattern synthesis. *J. Electromagn. Waves Appl.* **2018**, *32*, 1601–1615. [\[CrossRef\]](#)
12. Anjaneyulu, G.; Siddhartha Varma, J. Synthesis of Low Sidelobe Radiation Patterns from Embedded Dipole Arrays Using Genetic Algorithm. *Sustain. Commun. Netw. Appl.* **2020**, *39*, 791–797.
13. Mohammadi Shirkolaei, M. A New Design Approach of Low-Noise Stable Broadband Microwave Amplifier Using Hybrid Optimization Method. *IETE J. Res.* **2022**, *68*, 4160–4166. [\[CrossRef\]](#)
14. Khodier, M.M.; Christodoulou, C.G. Linear array geometry synthesis with minimum sidelobe level and null control using particle swarm optimization. *IEEE Trans. Antennas Propag.* **2005**, *53*, 2674–2679. [\[CrossRef\]](#)
15. Yan, K.; Lu, Y. Sidelobe reduction in array-pattern synthesis using genetic algorithm. *IEEE Trans. Antennas Propag.* **1997**, *45*, 1117–1122.
16. Kang, M.S.; Won, Y.J.; Lim, B.G.; Kim, K.T. Efficient Synthesis of Antenna Pattern Using Improved PSO for Spaceborne SAR Performance and Imaging in Presence of Element Failure. *IEEE Sensors J.* **2018**, *18*, 6576–6587. [\[CrossRef\]](#)
17. Cui, C.Y.; Jiao, Y.C.; Zhang, L. Synthesis of Some Low Sidelobe Linear Arrays Using Hybrid Differential Evolution Algorithm Integrated With Convex Programming. *IEEE Antennas Wirel. Propag. Lett.* **2017**, *16*, 2444–2448. [\[CrossRef\]](#)
18. Das, A.; Mandal, D.; Ghoshal, S.P.; Kar, R. Moth flame optimization based design of linear and circular antenna array for side lobe reduction. *Int. J. Numer. Model. Electron. Netw. Devices Fields* **2018**, *32*, e2486. [\[CrossRef\]](#)

19. Darvish, A.; Ebrahimzadeh, A. Improved Fruit-Fly Optimization Algorithm and Its Applications in Antenna Arrays Synthesis. *IEEE Trans. Antennas Propag.* **2018**, *66*, 1756–1766. [\[CrossRef\]](#)
20. Zheng, T. IWORMLF: Improved Invasive Weed Optimization With Random Mutation and Lévy Flight for Beam Pattern Optimizations of Linear and Circular Antenna Arrays. *IEEE Access* **2020**, *8*, 19460–19478. [\[CrossRef\]](#)
21. Li, X.; Luk, M.K. The Grey Wolf Optimizer and Its Applications in Electromagnetics, in IEEE Transactions on Antennas and Propagation. *J. Korean Inst. Commun. Inf. Sci.* **2020**, *68*, 2186–2197.
22. Zhang, H.; Liu, Z.; Gui, S.; Zou, M.; Wang, P. Improved mayfly algorithm based on hybrid mutation. *Electron. Lett.* **2022**, *58*, 687–689. [\[CrossRef\]](#)
23. Pinchera, D.; Migliore, M.D.; Schettino, F.; Lucido, M.; Panariello, G. An Effective Compressed-Sensing Inspired Deterministic Algorithm for Sparse Array Synthesis. *IEEE Trans. Antennas Propag.* **2018**, *66*, 149–159. [\[CrossRef\]](#)
24. Singh, U.; Kumar, H.; Kamal, T.S. Design of Yagi-Uda Antenna Using Biogeography Based Optimization. *IEEE Trans. Antennas Propag.* **2010**, *58*, 3375–3379. [\[CrossRef\]](#)
25. Baumgartner, P. Multi-Objective Optimization of Yagi-Uda Antenna Applying Enhanced Firefly Algorithm With Adaptive Cost Function. *IEEE Trans. Magn.* **2018**, *54*, 1–4. [\[CrossRef\]](#)
26. Quevedo-Teruel, O.; Rajo-Iglesias, E. Ant Colony Optimization in Thinned Array Synthesis With Minimum Sidelobe Level. *IEEE Antennas Wirel. Propag. Lett.* **2006**, *5*, 349–352. [\[CrossRef\]](#)
27. Zervoudakis, K.; Tsafarakis, S. *A Mayfly Optimization Algorithm*; Elsevier: Amsterdam, The Netherlands, 2020; Volume 145.
28. Owuola, E.O.; Xia, K.; Wang, T.; Umar, A.; Akindele, R.G. Pattern Synthesis of Uniform and Sparse Linear Antenna Array Using Mayfly Algorithm. *IEEE Access* **2021**, *9*, 77954–77975. [\[CrossRef\]](#)
29. Liu, Y.; Cao, B. A Novel Ant Colony Optimization Algorithm With Levy Flight. *IEEE Access* **2020**, *8*, 67205–67213. [\[CrossRef\]](#)
30. Zhang, J.; Wang, J.S. Improved Whale Optimization Algorithm Based on Nonlinear Adaptive Weight and Golden Sine Operator. *IEEE Access* **2020**, *8*, 77013–77048. [\[CrossRef\]](#)
31. Ho, Y.; Pepyne, D. Simple Explanation of the No-Free-Lunch Theorem and Its Implications. *J. Optim. Theory Appl.* **2002**, *115*, 549–570. [\[CrossRef\]](#)
32. Greda, L.A.; Winterstein, A.; Lemes, D.L.; Heckler, V.T. Beamsteering and Beamshaping Using a Linear Antenna Array Based on Particle Swarm Optimization. *IEEE Access* **2019**, *7*, 141562–141573. [\[CrossRef\]](#)
33. Sun, G.; Liu, Y.; Li, H.; Liang, S.; Wang, A.; Li, B. An antenna array sidelobe level reduction approach through invasive weed optimization. *Int. J. Antennas Propag.* **2018**, *2018*, 4867851–4867867. [\[CrossRef\]](#)
34. Mohammadi Shirkolaei, M.; Ghalibafan, J. Magnetically scannable slotted waveguide antenna based on the ferrite with gain enhancement. *Waves Random Complex Media* **2021**, *2021*, 1–11. [\[CrossRef\]](#)
35. Mohammadi Shirkolaei, M.; Dalili Oskoue, H.R.; Abbasi, M. Design of 1*4 Microstrip Antenna Array on the Human Thigh with Gain Enhancement. *IETE J. Res.* **2021**, 1–7. [\[CrossRef\]](#)

Disclaimer/Publisher’s Note: The statements, opinions and data contained in all publications are solely those of the individual author(s) and contributor(s) and not of MDPI and/or the editor(s). MDPI and/or the editor(s) disclaim responsibility for any injury to people or property resulting from any ideas, methods, instructions or products referred to in the content.